A Fast and Fixed Switching Frequency Model Predictive Control With Delay Compensation for Three-Phase Inverters

YONG YANG[1], (Member, IEEE), HUIQING WEN[2], (Member, IEEE), AND DEPENG LI[3]

[1]Soochow University, Suzhou 215137, China
[2]Xi'an Jiaotong-Liverpool University, Suzhou 215123, China
[3]University of Hawaii at Manoa, Honolulu, HI 96822 USA

Corresponding author: Huiqing Wen (huiqing.wen@xjtlu.edu.cn)

ABSTRACT Finite control set-model predictive control (FCS-MPC) has been used in power converters due to its advantages, such as fast dynamics, multi-objective control, and easy implement. However, due to variable switching frequency, the harmonics of inverter output current spread in a wide range of frequency. Furthermore, a large amount of computation is required for the implementation of the traditional FCS-MPC method. Here, an improved FCS-MPC algorithm with fast computation and fixed switching frequency is proposed in this paper for two-level three-phase inverters. First, according to the principle of deadbeat control, the inverter voltage vector reference can be constructed. Then, the operation durations and sequences of different voltage vectors are determined according to the location of the inverter voltage vector reference and the cost functions of different voltage vectors. In this algorithm, the operation durations of different voltage vectors are arranged inversely proportional to their cost functions. Compared with the conventional fixed switching frequency FCS-MPC control, the number of sectors involved in the FCS-MPC calculation can be reduced from 6 to 1, which greatly improves the computation efficiency. Moreover, the delay due to digital implementation is effectively compensated in the proposed algorithm. Finally, experimental tests are carried out to verify the advantages of the proposed method in terms of both steady-state and dynamic performance.

INDEX TERMS Finite control set-model predictive control (FCS-MPC), harmonics, fixed switching frequency, cost function, deadbeat control, delay compensation.

NOMENCLATURE

u_{aN}	Inverter output voltage of phase A
u_{bN}	Inverter output voltage of phase B
u_{cN}	Inverter output voltage of phase C
u_a	a component of inverter output voltage
u_β	β component of inverter output voltage
i_a	Inverter output current of phase A
i_b	Inverter output current of phase B
i_c	Inverter output current of phase C
i_a	a component of inverter output current
i_β	β component of inverter output current
V_{dc}	Dc-link voltage
E_{dc}	Dc power supply voltage
R_{dc}	Equivalent resistor of the dc input side
$S_{j=a,b,c}$	Switching states
L	Filter inductance
R	Loads
u_{Nn}	Neutral point voltage

I. INTRODUCTION

Due to the increasing awareness for environmental problems, renewable energy sources such as photovoltaic, wind and biomass power generation have been widely used nowadays. As the interface between renewable energy sources and loads or power grids, inverters act as the core of the renewable energy generation system and they directly affect the performance of the whole distributed generation systems [1]–[6].

According to the circuit structure, inverters can be usually divided into voltage-source inverters and current-source

inverters. Two-level voltage-source inverters are widely used in renewable energy generation systems due to its simple control. Many control strategies have been proposed in order to improve the performance of the two-level voltage-source inverters. Among these control strategies, voltage oriented control (VOC) and direct power control (DPC) are two widely used control schemes. For the VOC scheme, good steady-state and dynamic performance can be obtained. However, the tune of the proportional integral (PI) parameters is a tedious process [7], [8]. Furthermore, the control implementation is complicated. For DPC control, it can directly set the voltage vectors according to the power errors between the power references and the actual power [9], [10]. The dynamic performance can be improved. However, the inverter output current harmonics are large. Thus, high sampling frequency is essential in order to reduce the current harmonics and achieve good steady-state performance. Furthermore, due to variable switching frequency, harmonics of inverter output current spread in a wide range of frequency, which makes the filter design difficult.

In order to address above mentioned issues, model predictive control (MPC) was proposed, which shows lots of advantages such as simple control and multi-objective control. Considering the specific applications, the MPC algorithm has been further developed, such as continuous model-predictive control and finite control set-model predictive control (FCS-MPC). The FCS-MPC is widely used and the basic principle is to construct a multi-objective optimization cost function in order to judge the inverter's states and determine the appropriate switching combinations [11]–[21]. Specifically, the switching states that can result in the minimum cost function will be chosen and applied in the next switching cycle. The FCS-MPC algorithm shows advantages of easy implementing and the online optimization because the optimal switching states can be directly determined according to the minimal cost function [11]–[21]. Thus, the FCS-MPC algorithm has been widely used in many applications, such as three-phase grid-connected inverters, motor drives, multilevel converters and matrix converters especially with the quick developing of high performance digital signal processor (DSP) [11]–[21]. However, the output ripple by using the FCS-MPC is large since only one voltage vector is used per every control period. Furthermore, the output voltage and current harmonics spread in a wide range of frequency due to the variable switching frequency of the FCS-MPC, thus, the filter design becomes difficult [22]–[26].

Many strategies have been proposed to improve the performance of the FCS-MPC strategy. For instance, an online optimizing duty cycle control was proposed for three-phase active-front-end rectifiers [22], where a constant switching frequency was achieved in the FCS-MPC and the harmonic spectrum of the inverter output currents concentrated on multiple switching frequencies. However, this method is complex since instantaneous current variations need to calculate in the determination of different voltage vectors. To address variable switching frequency of the FCS-MPC,

an optimal switching sequences direct power control was proposed in [23], which accomplishes a constant switching frequency FCS-MPC control for two-level grid-connected converters. In [24], a multiple-vector direct model predictive power control was proposed for the grid-side back-to-back converter control. However, both methods discussed in [23] and [24] actually show heavy computational burden and occupy large computing resources. Similar researches can be found in [25] and [26], where FCS-MPC algorithms with fixed switching frequency have been used in H-bridge back-back converters and matrix converters respectively. However, both shows heavy computation burden considering the practical implementation.

Considering the renewable energy applications, the computation burden of FCS-MPC method needs to relieve in order to meet the inverter design requirements such as fast response and good steady-state performance. For instance, the code implementation duration of FCS-MPC algorithm should not occupy large percentage of switching period in order to accommodate other functions such as phase-locked loop, islanding detection protection, or maximum power point tracking algorithm, which are commonly required for grid-connected distributed generators. Usually the implementation duration is expected to limit within $100 \ \mu s$ for the IGBT-based inverters. However, when FCS-MPC algorithms are practically implemented in DSP, the online calculation of the predictive model and the cost function evaluation are necessary in order to online search the optimal voltage vectors, which will be time-consuming. For example, at least $52 \ \mu s$ is estimated to implement the FCS-MPC algorithm for the three-level three-phase inverters [27]. Therefore, in order to achieve a satisfied inverter response speed and output current waveform, it is essential to effectively relieve the computational burden of the algorithm especially the burden for predictive model and online optimization [28]. To address this, many algorithms have been proposed [29]–[31]. For instance, a low-complexity FSC-MPC with quick voltage selection and fast duty cycle calculation was proposed in [29] for three-phase two-level converter. It requires only one-step prediction to directly allocate the best voltage vector. Another fast FCS-MPC algorithm for multilevel cascaded H-bridge converter was presented, which can effectively reduce computation burden [30]. In [31], a FCS-MPC-based deadbeat solution for three-phase two-level inverter was presented, which may relieve the calculation burden compared with the traditional FCS-MPC. However, all these algorithms adopt a variable switching frequency, which will result in the spread of the converter output voltages or currents harmonics in a wide range of frequency.

In order to reduce the output harmonics, fixed switching frequency seems necessary. This paper presents an improved FCS-MPC with fast computation and fixed switching frequency, which shows advantages in the two-level voltage-source three-phase inverters. Firstly, the voltage vector reference can be constructed with a deadbeat control. Then, different voltage vectors are determined and effectively

applied in the predictive model and cost function optimization. With the proposed algorithm, the number of sectors involving in calculation of FCS-MPC is reduced from 6 to 1, which greatly improves the calculation efficiency. Furthermore, in order to reduce the influence of the digital control delay, the delay compensation is adopted in the proposed FCS-MPC with two step prediction. Finally, an experimental platform of a two-level voltage-source three-phase inverter was constructed. Both steady-state and dynamic experimental results are provided to verify the effectiveness of the proposed method.
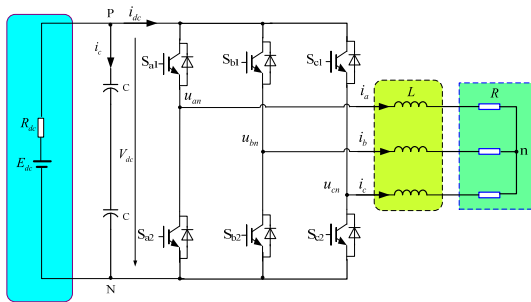

FIGURE 1. Structure of two-level three-phase inverter generation system.

II. PRINCIPLE OF THE PROPOSED FCS-MPC

A. MATHEMATICAL MODEL OF TWO-LEVEL THREE-PHASE INVERTERS

The two-level three-phase inverter topology for renewable energy power generation application is shown in Fig.1. This system contains renewable energy sources (such as photovoltaic, wind power), a two-level three-phase inverter, filter inductances and loads. In this system, the renewable energy source can be represented by the dc power supply E_{dc} containing the dc input equivalent resistor R_{dc}. The two-level three-phase inverter will transform the output dc power produced by E_{dc} to the load. As shown in Fig.1, u_{aN}, u_{bN} and u_{cN} represent the inverter output voltages, i_a, i_b and i_c represent the inverter output currents, L is filter inductance, V_{dc} is the dc-link bus voltage and R is the load.

According to different switching combinations, each phase of two-level three-phase inverters shown in Fig.1 has two operation statuses, which can be represented by "P" and "N". Take phase A as an example, switching state "P" means that the switch S_{a1} is on and the switch S_{a2} is off, thus the output voltage of phase A with respect to the point N is V_{dc}. Switching state "N" indicates that the switch S_{a1} is off and the switch S_{a2} is on, thus, the output voltage of phase A with respect to the point N is zero. Assuming the variables S_a, S_b and S_c represent the switching states of each phase, where "1" stands for the inverter output connected to the positive dc-link voltage, and "0" means that the inverter output is connected to the negative dc-link voltage. Switching states of two-level three-phase inverters can be represented by $S_j = [S_a S_b S_c]^T$, with $j = 0, \ldots, 7$. According to output switching combinations, totally 8 voltage vectors can

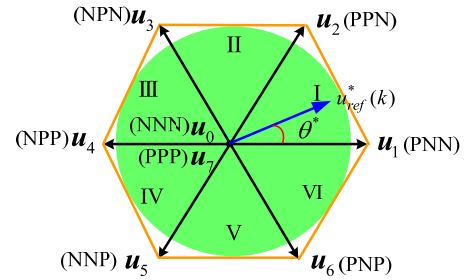be generated. Voltage vectors generated by the inverter are illustrated in Fig.2.

FIGURE 2. Output voltage vectors for two-level three-phase inverters.

The output phase voltages u_{aN}, u_{bN} and u_{cN} with respect to the point N can be expressed as:

$$\begin{bmatrix} u_{aN} \\ u_{bN} \\ u_{cN} \end{bmatrix} = \begin{bmatrix} S_a \\ S_b \\ S_c \end{bmatrix} V_{dc} \qquad (1)$$

For three-phase balanced systems, the voltage u_{Nn} between the dc-link negative point N and the load neutral point n can be derived as:

$$u_{Nn} = -\frac{u_{aN} + u_{bN} + u_{cN}}{3} \qquad (2)$$

Thus, the inverter output voltage u_{an}, u_{bn} and u_{cn} with respect to the point n can be derived as:

$$\begin{bmatrix} u_{an} \\ u_{bn} \\ u_{cn} \end{bmatrix} = \begin{bmatrix} u_{aN} \\ u_{bN} \\ u_{cN} \end{bmatrix} + \begin{bmatrix} u_{Nn} \\ u_{Nn} \\ u_{Nn} \end{bmatrix} \qquad (3)$$

According to current reference direction in Fig.1, the inverter output currents of the two-level three-phase inverter can be expressed as:

$$\begin{cases} L\dfrac{di_a}{dt} = u_{an} - Ri_a \\ L\dfrac{di_b}{dt} = u_{bn} - Ri_b \\ L\dfrac{di_c}{dt} = u_{cn} - Ri_c \end{cases} \qquad (4)$$

By combining (1), (2), (3) and (4), the output currents of the inverter can be calculated as:

$$\frac{d}{dt}\begin{bmatrix} i_a \\ i_b \\ i_c \end{bmatrix} = \frac{V_{dc}}{3L}\begin{bmatrix} 2 & -1 & -1 \\ -1 & 2 & -1 \\ -1 & -1 & 2 \end{bmatrix}\begin{bmatrix} S_a \\ S_b \\ S_c \end{bmatrix} + \frac{R}{L}\begin{bmatrix} i_a \\ i_b \\ i_c \end{bmatrix} \qquad (5)$$

From the equation (5), it can be found that the inverter output currents can be obtained by different inverter switching states and the dc-link voltage.

The mathematic model of the three-phase inverter in three-phase static *abc* reference frame needs to be transformed into the static *αβ* reference frame and the corresponding transformation matrix $C_{3/2}$ (invariant amplitude transformation) can

be written by

$$C_{3/2} = \frac{2}{3} \begin{bmatrix} 1 & -1/2 & -1/2 \\ 0 & \sqrt{3}/2 & -\sqrt{3}/2 \\ 1/\sqrt{2} & 1/\sqrt{2} & 1/\sqrt{2} \end{bmatrix} \quad (6)$$

Combination (4), (5) and (6), it can be derived as:

$$\begin{cases} L\dfrac{di_\alpha}{dt} = u_{\alpha n} - Ri_\alpha \\ L\dfrac{di_\beta}{dt} = u_{\beta n} - Ri_\beta \end{cases} \quad (7)$$

where i_a and i_β represent the *a* component of the output current and the *β* component of the output current in the *αβ* reference frame, respectively. u_a and u_β are the *a* component of the output voltage and the *β* component of the output voltage in the *αβ* reference frame, respectively.

Assuming the sampling time is relatively small, the discretization of (7) by using forward Euler approximation can be derived as:

$$\begin{cases} L\dfrac{i_\alpha(k+1) - i_\alpha(k)}{T_s} = u_{an}(k) - Ri_\alpha(k) \\ L\dfrac{i_\beta(k+1) - i_\beta(k)}{T_s} = u_{\beta n}(k) - Ri_\beta(k) \end{cases} \quad (8)$$

where T_s is the sampling time.

The future load currents at the (k+1)th instant can be predicted by using (8) as:

$$\begin{cases} i_\alpha(k+1) = \dfrac{T_s}{L}[u_{an}(k) - Ri_\alpha(k)] + i_\alpha(k) \\ i_\beta(k+1) = \dfrac{T_s}{L}[u_{\beta n}(k) - Ri_\beta(k)] + i_\beta(k) \end{cases} \quad (9)$$

According to the deadbeat control, the inverter output currents will reach their references in one sampling period and can be expressed as:

$$\begin{cases} i_\alpha(k+1) = i_\alpha^*(k+1) \\ i_\beta(k+1) = i_\beta^*(k+1) \end{cases} \quad (10)$$

In order to achieve the inverter currents tracking with respect to the reference in the next sampling time, the inverter desired output voltages in the *αβ* coordinate reference can be obtained by using (9) and (10) as:

$$\begin{cases} u_{\alpha n}^*(k) = \dfrac{L}{T_s}[i_\alpha^*(k+1) - i_\alpha(k)] + Ri_\alpha(k) \\ u_{\beta n}^*(k) = \dfrac{L}{T_s}[i_\beta^*(k+1) - i_\beta(k)] + Ri_\beta(k) \end{cases} \quad (11)$$

where $u_{an}^*(k)$ and $u_{\beta n}^*(k)$ are the *a* component and *β* component of the desired output voltages at the (*k*)th instant.

B. DELAY TIME COMPENSATION

With the model predictive control, the time sequence can be illustrated in Fig.3. At the (*k*)th sampling time, the inverter currents are sampled with analog to digital converter (ADC), and at t_1, the ADC process is completed. At t_2, main algorithms will be implemented, thus, the operation times and sequences of different voltage vectors can be determined. Then, the switching signals for power electronic devices of

the inverter are generated at the (k + 1)th instant. Therefore, voltage vectors adopted at the (k)th instant will be updated and applied for the (k + 1)th instant.

In order to eliminate the control delay due to the digital implementation, the voltage vectors need to be determined at the (k + 1)th instant [16], [32], [33]. By time shifting (11) one step forward, the predictive voltage model can be obtained as:

$$\begin{cases} u_{\alpha n}^*(k+1) = \dfrac{L}{T_s}[i_\alpha^*(k+2) - i_\alpha(k+1)] + Ri_\alpha(k+1) \\ u_{\beta n}^*(k+1) = \dfrac{L}{T_s}[i_\beta^*(k+2) - i_\beta(k+1)] + Ri_\beta(k+1) \end{cases}$$
$$(12)$$

Combining (9) and (12), it can be derived as:

$$\begin{cases} u_{\alpha n}^*(k+1) = \dfrac{L}{T_s}[i_\alpha^*(k+2) - i_\alpha(k)] \\ \qquad + (2 - \dfrac{RT_s}{L})Ri_\alpha(k) + (\dfrac{RT_s}{L} - 1)u_{\alpha n}(k) \\ u_{\beta n}^*(k+1) = \dfrac{L}{T_s}[i_\beta^*(k+2) - i_\beta(k)] \\ \qquad + (2 - \dfrac{RT_s}{L})Ri_\beta(k) + (\dfrac{RT_s}{L} - 1)u_{\beta n}(k) \end{cases}$$
$$(13)$$

where $u_{an}(k)$ and $u_{\beta n}(k)$ are the *a* component and *β* component of selected voltage vectors at the previous instant.

The *a* component of the current reference $i_a^*(k+1)$ and the *β* component of the current reference $i_\beta^*(k+1)$ at the (k + 1)th instant can be constructed by the values at the present, one past and two past current references according to linear interpolation theorem. Thus,

$$\begin{cases} i_\alpha^*(k+1) = 3i_\alpha^*(k) - 3i_\alpha^*(k-1) + i_\alpha^*(k-2) \\ i_\beta^*(k+1) = 3i_\beta^*(k) - 3i_\beta^*(k-1) + i_\beta^*(k-2) \end{cases} \quad (14)$$

Similarly, the *a* component current reference $i_a^*(k+2)$ and the *β* component current reference $i_\beta^*(k+2)$ at the (k + 2)th instant can be obtained as:

$$\begin{cases} i_\alpha^*(k+2) = 3i_\alpha^*(k+1) - 3i_\alpha^*(k) + i_\alpha^*(k-1) \\ i_\beta^*(k+2) = 3i_\beta^*(k+1) - 3i_\beta^*(k) + i_\beta^*(k-1) \end{cases} \quad (15)$$

C. ALGORITHM PRINCIPLE

In order to achieve fast and accurate tracking of given currents, the current tracking cost function of the conventional FCS-MPC based on voltage model can be expressed as [31]:

$$g = \left| u_{\alpha n}^*(k+1) - u_{\alpha n}(k+1) \right| + \left| u_{\beta n}^*(k+1) - u_{\beta n}(k+1) \right|$$
$$(16)$$

where $u_{an}(k+1)$ and $u_{\beta n}(k+1)$ represent the inverter voltage vectors to be applied.

According to (3), (6) and the inverter switching states, the inverter voltage vectors $u_{an}(k+1)$ and $u_{\beta n}(k+1)$ can be derived as:

$$\begin{bmatrix} u_{\alpha n}(k+1) \\ u_{\beta n}(k+1) \end{bmatrix} = \frac{2}{3}V_{dc} \begin{bmatrix} 1 & -1/2 & -1/2 \\ 0 & \sqrt{3}/2 & -\sqrt{3}/2 \end{bmatrix} \begin{bmatrix} S_a(k+1) \\ S_b(k+1) \\ S_c(k+1) \end{bmatrix}$$
$$(17)$$

where $S_a(k+1)$, $S_b(k+1)$ and $S_c(k+1)$ represent the inverter switching states at the (k + 1)th instant, respectively.

According to (13), (16) and (17), it can be found that the predictive model and the cost function adopted by the traditional FCS-MPC require on-line calculation and evaluation for all these eight voltage vectors. With the rule to achieve the minimum cost function, the voltage vector for the next control cycle is chosen. With the conventional FCS-MPC, the output current ripple of the inverter is large and harmonics spread in a wide range of frequency. In order to set the harmonic spectrum of the inverter currents fixed at multiple switching frequencies, the proposed FCS-MPC with fixed switching frequency is used. Taking the first sector as example, as illustrated in Fig.2, the current tracking cost function g for the active voltage vectors u_1, u_2 and zero voltage vectors u_0 or (u_7) are g_{1a}, g_{1b}, and g_{1c}, respectively. The operation time for the voltage vectors u_1, u_2 and u_0 or (u_7) in each control cycle is t_{1a}, t_{1b} and t_{1c}, respectively. Since the operation time for each voltage vector is inversely proportional to the cost function, larger current tracking cost function leads to smaller operation time for each voltage vector. Thus, the operation time of different voltage vectors can be derived as:

$$\begin{cases} t_{1a} = T_s(1/g_{1a})/((1/g_{1a}) + (1/g_{1b}) + (1/g_{1c})) \\ t_{1b} = T_s(1/g_{1b})/((1/g_{1a}) + (1/g_{1b}) + (1/g_{1c})) \\ t_{1c} = T_s(1/g_{1c})/((1/g_{1a}) + (1/g_{1b}) + (1/g_{1c})) \\ T_s = t_{1a} + t_{1b} + t_{1c} \end{cases} \quad (18)$$

Note that each operation time lies within the range $[0, T_s]$. By using the FCS-MPC with the fixed switching frequency, the sector cost function in the first sector can be expressed by

$$G_1 = \frac{t_{1a}}{T_s}g_{1a} + \frac{t_{1b}}{T_s}g_{1b} + \frac{t_{1c}}{T_s}g_{1c} \quad (19)$$

Similarly, the operation time of different voltage vectors can be derived. For example, define the current tracking cost functions for the active voltage vectors u_2, u_3 and the zero voltage vectors u_0 or (u_7) are g_{2a}, g_{2b} and g_{2c}, respectively. Also, the operation times for u_2, u_3 and u_0 or (u_7) in each control cycle are t_{2a}, t_{2b} and t_{2c}, respectively. The operation time for different voltage vectors in the sector 2 can be expressed by

$$\begin{cases} t_{2a} = T_s(1/g_{2a})/((1/g_{2a}) + (1/g_{2b}) + (1/g_{2c})) \\ t_{2b} = T_s(1/g_{2b})/((1/g_{2a}) + (1/g_{2b}) + (1/g_{2c})) \\ t_{2c} = T_s(1/g_{2c})/((1/g_{2a}) + (1/g_{2b}) + (1/g_{2c})) \\ T_s = t_{2a} + t_{2b} + t_{2c} \end{cases} \quad (20)$$

The sector cost function for the sector 2 can be expressed as:

$$G_2 = \frac{t_{2a}}{T_s}g_{2a} + \frac{t_{2b}}{T_s}g_{2b} + \frac{t_{2c}}{T_s}g_{2c} \quad (21)$$

Similarly, the sector cost functions for the sector 3, 4, 5, and 6 can be obtained and denoted as G_3, G_4, G_5 and G_6, respectively. The sector which shows minimum sector cost
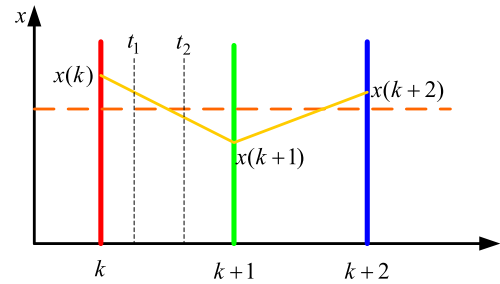

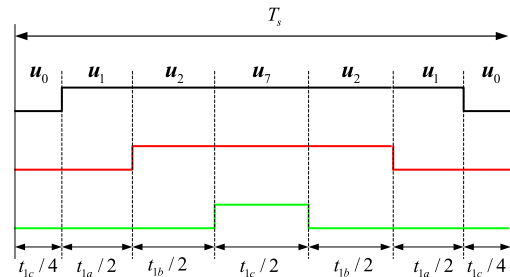**FIGURE 3.** Time sequences of the model predictive control as the digital controller.

FIGURE 4. Operation time and sequences of different voltage vectors for Sector 1.

function is selected and its voltage vectors will be used in the next control cycle [25], [26].

In order to reduce harmonics of the inverter output voltage and current, the operation time of different voltage vectors is symmetrically distributed. Zero voltage vectors u_0 and u_7 are utilized with the same operation time. In addition, in order to minimize the switching loss, only one-phase devices are switched at every switching period. Assume that the reference voltage vector is located in the sector 1, as illustrated in Fig.1, the sequence of operation voltage vectors is arranged as: NNN-PNN-PPN-PPP-PPN-PNN-NNN. Thus, the operation time and sequences of different voltage vectors are illustrated in Fig.4.

With the conventional fixed switching frequency FCS-MPC, for each of six sectors, the predictive model, the current tracking cost function, operation time and the sector cost function need to be calculated. Specifically, for each sector, two active voltage vectors and one zero voltage vector are required. Thus, the computational burden is high. In order to reduce computational load, a fast and fixed switching frequency FCS-MPC has been adopted. The candidate voltage vectors are determined according to the location of the reference voltage vector $u_{ref}^*(k+1) = u_{an}^*(k+1) + ju_{\beta n}^*(k+1)$ derived from the equation (13). For instance, if the reference voltage vector $u_{ref}^*(k+1)$ is located in sector 1, as illustrated in Fig.2, the operation time of candidate voltage vectors can be determined by (18). Furthermore, the operation sequences of different voltage vectors are arranged as Fig.4. Thus, the number of sectors involving FCS-MPC is reduced from 6 to 1, which greatly improves the computation efficiency.

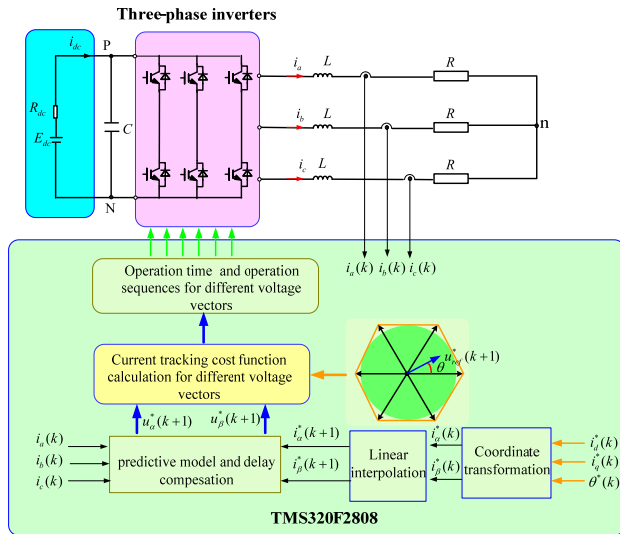In order to facilitate the control implementation, the inverter current references in static $\alpha\beta$ coordinate

FIGURE 5. Diagram of the proposed FCS-MPC control strategy for two-level three-phase inverters.

TABLE 1. Experimental parameters.

Parameter	Description	Values
E_{dc} (V)	Dc input voltage	200
R_{dc} (Ω)	Dc input equivalent resistor	0.1
ω^* (rad/s)	Given angular frequency	314.16
C (μF)	Dc-link bus capacitor	1000
R (Ω)	Loads	20
L (mH)	Filter inductance	12
f_s (kHz)	Sampling frequency	16
T_d (μs)	Dead time	2

reference are transformed into *dq* rotating coordinate reference and expressed as:

$$\begin{bmatrix} i_\alpha^* \\ i_\beta^* \end{bmatrix} = \begin{bmatrix} \cos\theta^* & -\sin\theta^* \\ \sin\theta^* & \cos\theta^* \end{bmatrix} \begin{bmatrix} i_d^* \\ i_q^* \end{bmatrix} \quad (22)$$

where i_α^* and i_β^* represent the *a* and *β* component current references of the inverter, i_d^* and i_q^* represent the inverter *d*-axis and *q*-axis current reference, θ^* represents the given value of phase angle and can be expressed as $\theta^* = \omega^* t$, ω^* is the given current angular frequency. Fig.5 illustrates the control strategy of the proposed FCS-MPC for two-level three-phase inverters.

III. EXPERIMENTAL RESULTS

In order to verify the effectiveness of the fast and fixed switching frequency FCS-MPC, experimental tests were carried out for both steady-state and transient conditions, and compared with the traditional FCS-MPC strategies. All strategies are implemented on a 32 bit DSP (TMS320F2808) from Texas Instruments. In the test, a programmable dc power supply is used to emulate renewable energy sources. Main experimental parameters are shown in Table 1.

A. COMPARISON OF EXECUTION TIME
In order to verify the effectiveness of the proposed FCS-MPC, execution time for three FCS-MPC strategies are compared.
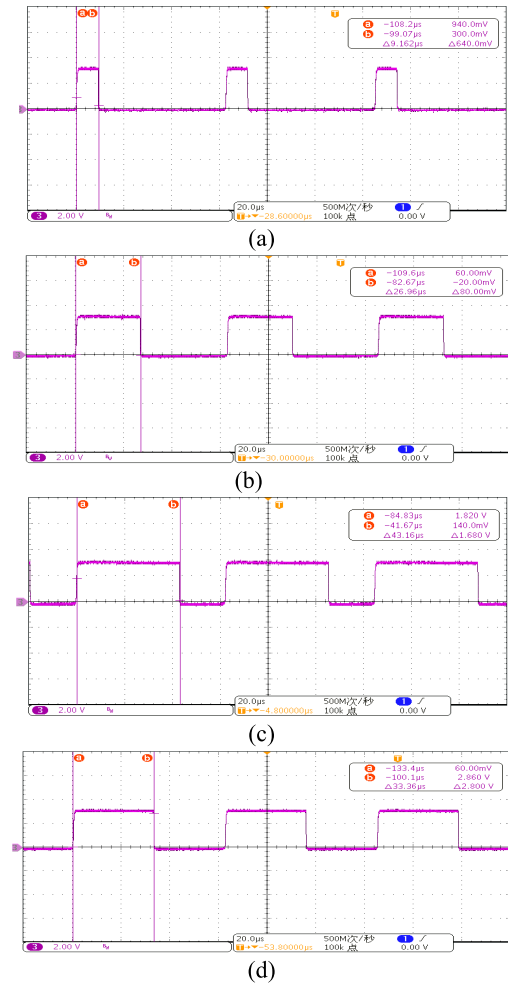

FIGURE 6. Execution time for different FCS-MPC strategies. (a) Execution time for ADC process and other auxiliary tasks; (b) Execution time with the traditional FCS-MPC; (c) Execution time with the fixed switching frequency FCS-MPC [26]; (d) Execution time with the proposed FCS-MPC.

These FCS-MPC strategies are: the traditional FCS-MPC method with only one voltage vector for each control cycle based on the cost function (16), fixed switching frequency FCS-MPC method discussed in [26], and the proposed FCS-MPC in this paper. In the test, an input/output (I/O) port of DSP is used to capture the duration of high level as the execution time of different FCS-MPC. The crystal frequency of a 32 bit DSP (TMS320F2808) is 100 M and the time interval is 62.25 μs. Fig.6 (a) shows the measured execution time for ADC process and other auxiliary tasks. Fig.6 (b) represents the measured execution time when executing with the traditional FCS-MPC. Fig.6 (c) shows the measured execution time with the fixed switching frequency FCS-MPC method discussed in [26]. Fig.6 (d) shows the measured execution time with the proposed FCS-MPC in this paper.
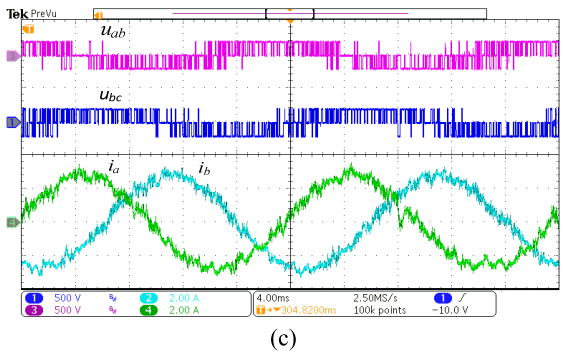
As shown in Fig.6, it takes about 9.2 μs to implement ADC process and other auxiliary tasks. The execution time for the classical FCS-MPC algorithm is about 17.8 μs (27 μs −9.2 μs). For the conventional fixed switching
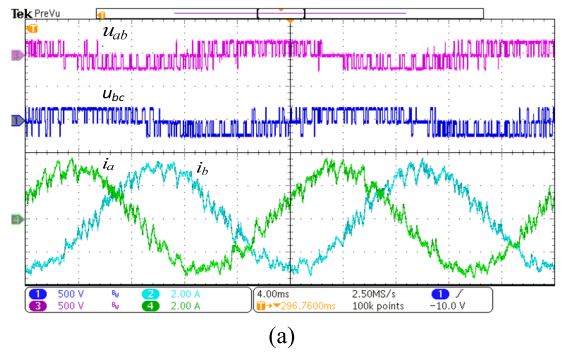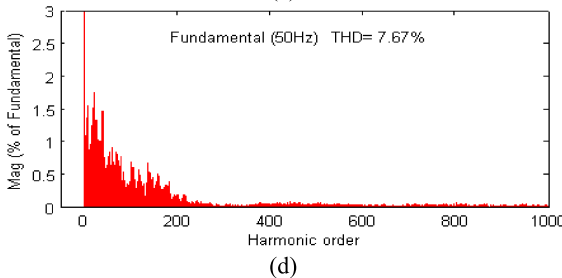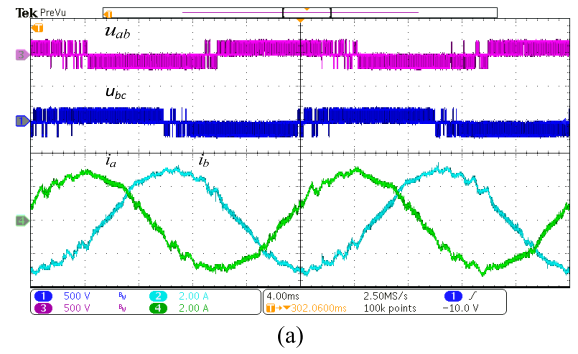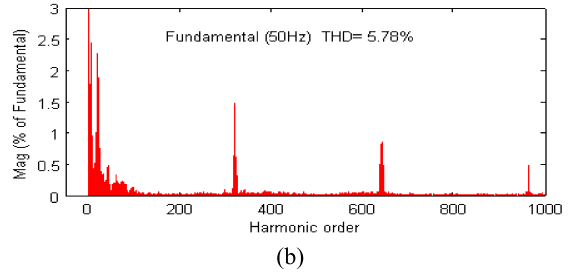
(a)
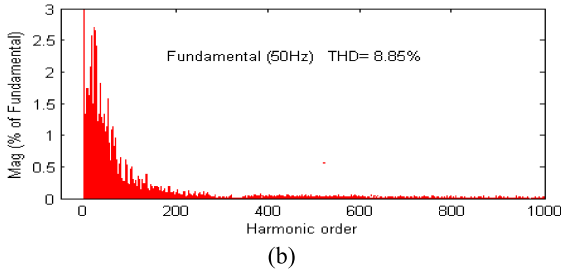
(b)

(c)

(d)

FIGURE 7. Steady-state experimental waveforms with the traditional FCS-MPC under case 1. (a) Output line voltage and current without delay compensation; (b) Phase A harmonic spectrum without delay compensation; (c) Output line voltage and current with delay compensation; (d) Phase A harmonic spectrum with delay compensation.

(a)

(b)

(c)

(d)

FIGURE 8. Steady-state experimental waveforms with the fixed switching frequency FCS-MPC [26] under case 1: (a) Output line voltage and current without delay compensation; (b) Phase A harmonic spectrum without delay compensation; (c) Output line voltages and currents with delay compensation; (d) Phase A harmonic spectrum with delay compensation.
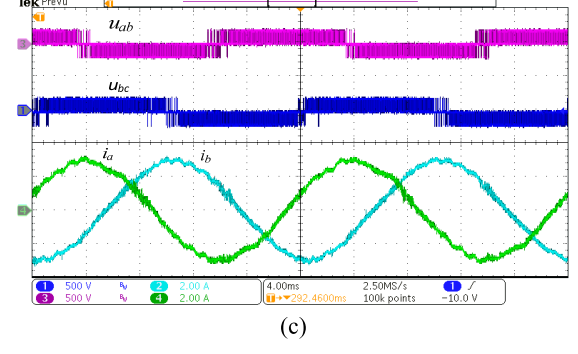
frequency FCS-MPC method, it needs about 34 μs (43.2 μs -9.2 μs), and it is only requiring about 24.2 μs (33.4 μs -9.2 μs) to execute the proposed fixed switching frequency FCS-MPC algorithm. From the above analysis, it can be concluded that the execution time of the classical FCS-MPC algorithm is shortest, and the execution time is about half of the execution time using the conventional fixed switching frequency FCS-MPC method. Compared with the two fixed switching frequency, the execution time of proposed method is about 71.2% of the execution time using
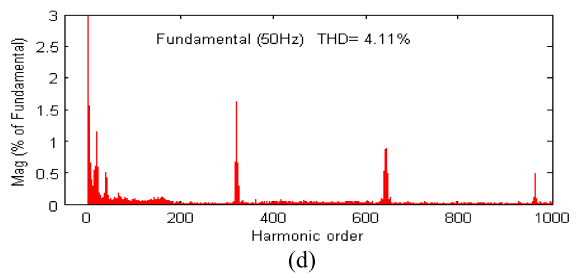
the classical fixed switching frequency FCS-MPC method, which greatly improves the computation efficiency.

B. STEADY-STATE RESULTS
For the steady-state performance evaluation, the experimental condition considered to evaluation three FCS-MPC algorithms is set as followings:

Case 1: The reference current for d-axis current and the q-axis current are set as $i_d^* = 4$ A and $i_q^* = 0$ A, respectively. And the inverter output current frequency is 50 Hz.
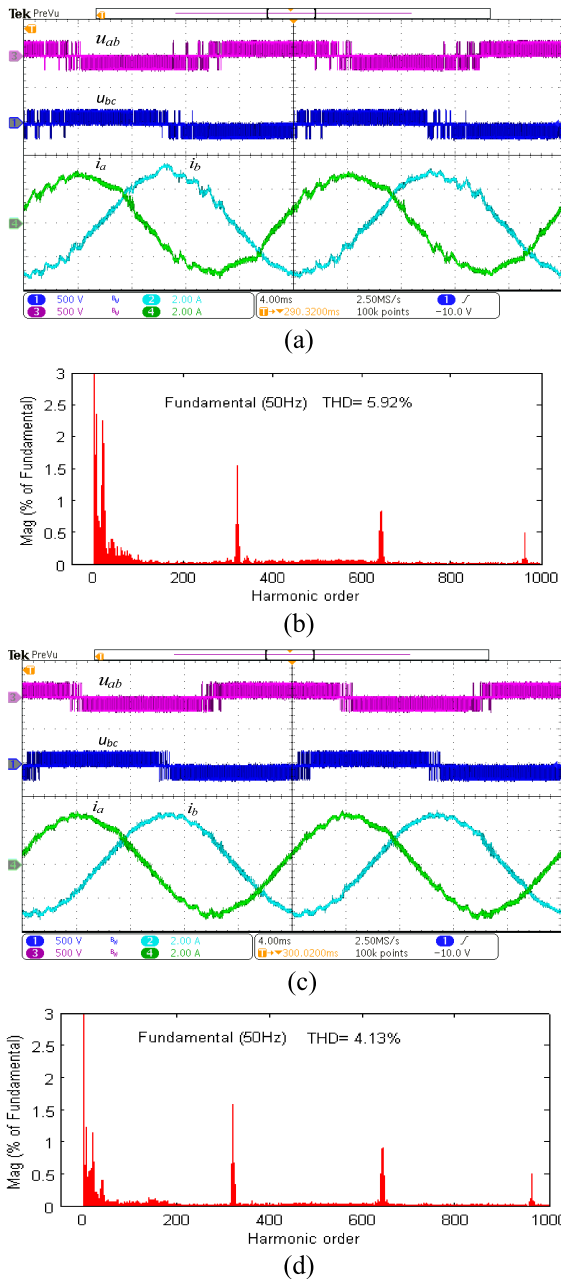
(a)

(b)

(c)

(d)

FIGURE 9. Steady-state experimental waveforms with the proposed FCS-MPC under case 1. (a) Output line voltage and current without delay compensation; (b) Phase A harmonic spectrum without delay compensation; (c) Output line voltage and current with delay compensation; (d) Phase A harmonic spectrum with delay compensation.

Fig.7 (a) shows the experimental waveforms of output line voltage u_{ab}, u_{bc}, phase currents i_a and i_b under case 1 when using the traditional FCS-MPC without delay compensation, and Fig.7 (c) shows the corresponding results with delay compensation. Fig.7 (b) and Fig.7 (d) show the harmonic spectrum of phase A current without delay compensation and with delay compensation, respectively. With the fixed switching frequency FCS-MPC [26], the corresponding results are illustrated in Fig.8. With the proposed FCS-MPC, the corresponding results are illustrated in Fig.9.
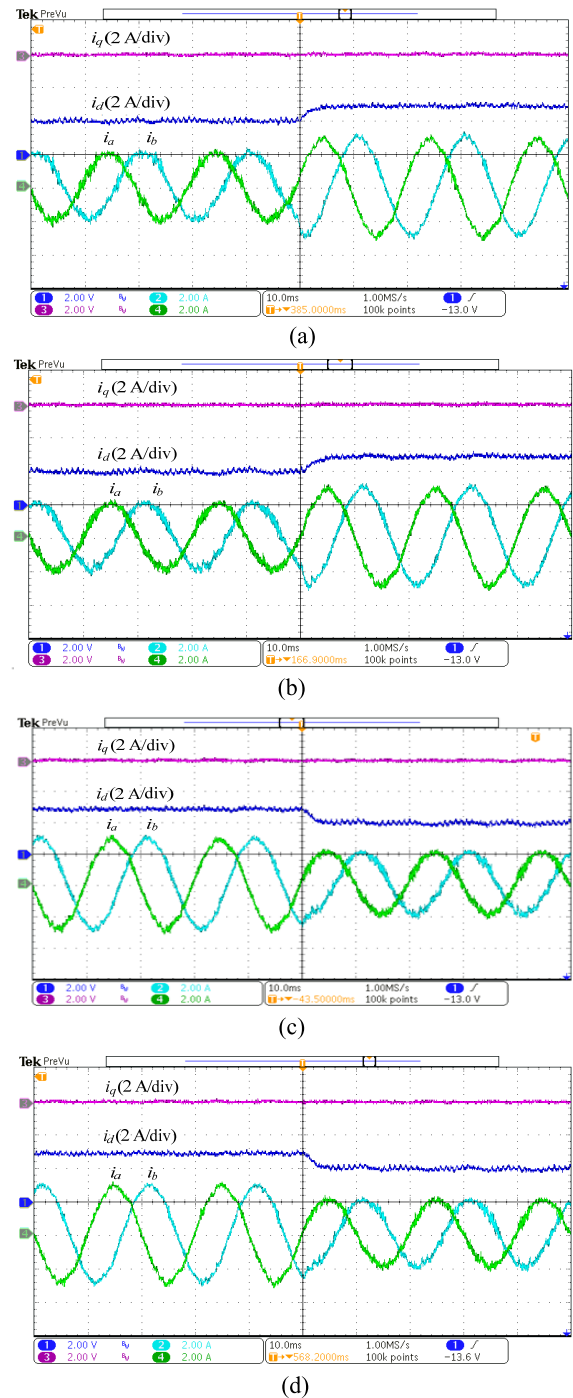

(a)

(b)

(c)

(d)

FIGURE 10. Dynamic experimental waveforms with different strategies: (a) the fixed switching frequency FCS-MPC [26] under case 2; (b) the proposed FCS-MPC under case 2; (c) the fixed switching frequency FCS-MPC [26] under case 3; (d) the proposed FCS-MPC under case 3.

The steady-state experimental results show that three different FCS-MPC algorithms with delay compensation improve the steady-state performance. Specifically, with the traditional FCS-MPC method, the total harmonic distortion (THD) of inverter phase A current is reduced from 8.85% to 7.67%. The corresponding THD of phase A current with the fixed switching frequency FCS-MPC algorithm [26] is reduced from 5.78% to 4.11%, and the corresponding THD of

phase A current is decreased from 5.92% to 4.13% by using the proposed FCS-MPC algorithm. These results show that all three methods can track the current references successfully with sinusoidal output currents. As shown in Fig.7, phase A current harmonic spectrum is scattered over different frequencies, which makes the filter design difficult. However, as illustrated in Fig.8 and Fig.9, with the fixed switching frequency FCS-MPC, the phase A current harmonic spectrum is mainly concentrated around the switching frequency and its multiple switching frequencies such as 16 kHz, 32 kHz and 48 kHz, which is very similar to using traditional space vector pulse width modulation (SVPWM) method and beneficial to the filter design. As displayed in Fig.8 and Fig.9, the two fixed switching frequency FCS-MPC methods show almost similar steady-state performance.

C. DYNAMIC RESULTS
In the dynamic performance evaluation, two test conditions are considered to evaluate the performance of the fixed switching frequency FCS-MPC algorithm [26] and the proposed FCS-MPC.

Case 2: The d-axis current reference is jumped from $i_d^* = 2.4$ A to $i_d^* = 4$ A, while the q-axis current reference and the output frequency of the inverter are kept constant as: $i_q^* = 0$ A and $f^* = 50$ Hz, respectively.

Case 3: The d-axis current reference is suddenly reduced from $i_d^* = 4$ A to $i_d^* = 2.4$ A, while the q-axis current reference and the output frequency of the inverter are kept the same with the case 2.

Fig.10 (a) and Fig.10 (b) show the experimental waveforms of d-axis current i_d, q-axis current i_q, phase currents i_a and i_b under case 2, respectively. Fig.10 (c) and Fig.10 (d) presents the corresponding results under case 3. Fig.10 (a) and Fig.10 (b) show that it takes about 4 ms to reach the given currents by using both fixed switching frequency FCS-MPC methods. As shown in Fig.10 (c) and Fig.10 (d), the d-axis and the q-axis current of the inverter achieve the current references within about 2 ms for a step change of current magnitude from 4 A to 2.4 A. As shown in Fig.10, both fixed switching frequency FCS-MPC methods show very good and almost similar dynamic performance.

IV. CONCLUSION
The paper presents a fast and fixed switching frequency FCS-MPC algorithm with delay compensation, which is applied in two-level three-phase inverters. Steady-state and dynamic experiments for three different FCS-MPC controls have been carried out, and the following conclusions are drawn:

(1)The proposed FCS-MPC control with delay compensation greatly improves steady-state performance.

(2)The proposed FCS-MPC control makes harmonic spectrum of output current of the inverter mainly concentrate around the switching frequency and its multiple switching frequencies.

(3) Compared with the traditional fixed switching FCS-MPC, the number of sectors involving in FCS-MPC is

reduced from 6 to 1, which greatly improves the computation efficiency.

(4) The inverter with the proposed FCS-MPC control has good steady-state and dynamic performance, and has almost similar performance compared with the classical fixed switching frequency FCS-MPC method.

In a word, the fast and fixed switching frequency FCS-MPC combines the advantages of the FCS-MPC and the SVPWM method. The proposed algorithm eases real-time implementation on industrial real-time platform due to greatly reduced computation time compared with the classical fixed switching frequency FCS-MPC. Therefore, the presented method has a good application prospect in distributed generation systems.

REFERENCES
[1] R. Teodorescu, M. Liserre, and P. Rodriguez, *Grid Converters for Photovoltaic and Wind Power Systems*, New York, NY, USA: Wiley, 2011.
[2] A. Camacho, M. Castilla, J. Miret, J. Vasquez, and E. Alarcon-Gallo, "Flexible voltage support control for three-phase distributed generation inverters under grid fault," *IEEE Trans. Ind. Electron.*, vol. 60, no. 4, pp. 1429–1441, Apr. 2013.
[3] A. Calle-Prado, S. Alepuz, J. Bordonau, J. Nicolas-Apruzzese, P. Cortés, and J. Rodriguez, "Model predictive current control of grid-connected neutral-point-clamped converters to meet low-voltage ride-through requirements," *IEEE Trans. Ind. Electron.*, vol. 62, no. 3, pp. 1503–1514, Mar. 2015.
[4] B. Cai, Y. Zhao, H. Liu, and M. Xie, "A data-driven fault diagnosis methodology in three-phase inverters for PMSM drive systems," *IEEE Trans. Power Electron.*, vol. 32, no. 7, pp. 5590–5600, Jul. 2017.
[5] B. Cai, L. Huang, and M. Xie, "Bayesian networks in fault diagnosis," *IEEE Trans. Ind. Informat.*, to be published.
[6] B. Cai *et al.*, "Multi-source information fusion based fault diagnosis of ground-source heat pump using Bayesian network," *Appl. Energy*, vol. 114, no. 2, pp. 1–9, Feb. 2014.
[7] A. Bouafia, J. P. Gaubert, and F. Krim, "Predictive direct power control of three-phase pulsewidth modulation (PWM) rectifier using space-vector modulation (SVM)," *IEEE Trans. Power Electron.*, vol. 25, no. 1, pp. 228–236, Jan. 2010.
[8] Y. Zhang and C. Qu, "Direct power control of a pulse width modulation rectifier using space vector modulation under unbalanced grid voltages," *IEEE Trans. Power Electron.*, vol. 30, no. 10, pp. 5892–5901, Oct. 2015.
[9] Y. Zhang and C. Qu, "Table-based direct power control for three-phase AC/DC converters under unbalanced grid voltages," *IEEE Trans. Power Electron.*, vol. 30, no. 12, pp. 7090–7099, Dec. 2015.
[10] J. Alonso-Martinez, J. E.-G. Carrasco, and S. Arnaltes, "Table-based direct power control: A critical review for microgrid applications," *IEEE Trans. Power Electron.*, vol. 25, no. 12, pp. 2949–2961, Dec. 2010.
[11] Y. Zhang and C. Qu, "Model predictive direct power control of PWM rectifiers under unbalanced network conditions," *IEEE Trans. Ind. Electron.*, vol. 62, no. 7, pp. 4011–4022, Jul. 2015.
[12] J. Rodriguez *et al.*, "State of the art of finite control set model predictive control in power electronics," *IEEE Trans. Ind. Informat.*, vol. 9, no. 2, pp. 1003–1016, May 2013.
[13] H. A. Young, M. A. Perez, J. Rodriguez, and H. Abu-Rub, "Assessing finite-control-set model predictive control: A comparison with a linear current controller in two-level voltage source inverters," *IEEE Ind. Electron. Mag.*, vol. 8, no. 1, pp. 44–52, Mar. 2014.
[14] M. Trabelsi, S. Bayhan, K. A. Ghazi, H. Abu-Rub, and L. Ben-Brahim, "Finite control set model predictive control for grid connected packed-U-cells multilevel inverter," *IEEE Trans. Ind. Electron.*, vol. 63, no. 11, pp. 7286–7295, Nov. 2016.
[15] V. Yaramasu, M. Rivera, M. Narimani, J. Rodriguez, and B. Wu, "Model predictive approach for a simple and effective load voltage control of four-leg inverter with an output LC filter," *IEEE Trans. Ind. Electron.*, vol. 61, no. 10, pp. 5259–5270, Oct. 2014.
[16] P. Cortes, J. Rodríguez, C. Silva, and A. Flores, "Delay compensation in model predictive current control of a three-phase inverter," *IEEE Trans. Ind. Electron.*, vol. 59, no. 2, pp. 1323–1325, Feb. 2012.

[17] M. Rivera, V. Yaramasu, A. Llor, J. Rodriguez, B. Wu, and M. Fadel, "Digital predictive current control of a three-phase four-leg inverter," *IEEE Trans. Ind. Electron.*, vol. 60, no. 11, pp. 4903–4912, Nov. 2013.

[18] M. Rivera, J. Rodriguez, B. Wu, J. Espinoza, and C. Rojas, "Current control for an indirect matrix converter with filter resonance mitigation," *IEEE Trans. Ind. Electron.*, vol. 59, no. 1, pp. 71–79, Jan. 2012.

[19] J. Scoltock, T. Geyer, and U. K. Madawala, "A comparison of model predictive control schemes for MV induction motor drives," *IEEE Trans. Ind. Informat.*, vol. 9, no. 2, pp. 909–919, May 2013.

[20] B. S. Riar, T. Geyer, and U. K. Madawala, "Model predictive direct current control of modular multilevel converters: Modeling, analysis, and experimental evaluation," *IEEE Trans. Power Electron.*, vol. 30, no. 1, pp. 431–439, Jan. 2015.

[21] M. Narimani, B. Wu, V. Yaramasu, Z. Cheng, and N. R. Zargari, "Finite control-set model predictive control (FCS-MPC) of nested neutral point-clamped (NNPC) converter," *IEEE Trans. Power Electron.*, vol. 30, no. 12, pp. 7269–7276, Dec. 2015.

[22] Z. Song, Y. Tian, W. Chen, Z. Zou, and Z. Chen, "Predictive duty cycle control of three-phase active-front-end rectifiers," *IEEE Trans. Power Electron.*, vol. 31, no. 1, pp. 698–710, Jan. 2016.

[23] S. Vazquez, A. Marquez, A. Aguilera, D. Quevedo, J. I. Leon, and L. G. Franquelo, "Predictive optimal switching sequence direct power control for grid-connected power converters," *IEEE Trans. Ind. Electron.*, vol. 62, no. 4, pp. 2010–2020, Apr. 2015.

[24] Z. Zhang, H. Fang, F. Gao, J. Rodriguez, and R. Kennel, "Multiple-vector model predictive power control for grid-tied wind turbine system with enhanced steady-state control performance," *IEEE Trans. Ind. Electron.*, vol. 64, no. 8, pp. 6287–6298, Aug. 2017.

[25] L. Tarisciotti, P. Zanchetta, A. Watson, S. Bifaretti, and J. C. Clare, "Modulated model predictive control for a seven-level cascaded H-bridge back-to-back converter," *IEEE Trans. Ind. Electron.*, vol. 61, no. 10, pp. 5375–5383, Oct. 2014.

[26] M. Vijayagopal, P. Zanchetta, L. Empringham, L. de Lillo, L. Tarisciotti, and P. Wheeler, "Control of a direct matrix converter with modulated model-predictive control," *IEEE Trans. Ind. Appl.*, vol. 53, no. 3, pp. 2342–2349, May 2017.

[27] R. Vargas, P. Cortes, U. Ammann, J. Rodriguez, and J. Pontt, "Predictive control of a three-phase neutral point clamped inverter," *IEEE Trans. Ind. Electron.*, vol. 54, no. 5, pp. 2697–2705, May 2007.

[28] J. D. Barros, J. F. A. Silva, and É. G. A. Jesus, "Fast-predictive optimal control of NPC multilevel converters," *IEEE Trans. Ind. Electron.*, vol. 60, no. 2, pp. 619–627, Feb. 2013.

[29] Y. Zhang and W. Xie, "Low complexity model predictive control—Single vector-based approach," *IEEE Trans. Power Electron.*, vol. 29, no. 10, pp. 5532–5541, Oct. 2014.

[30] Y. Zhang, X. Wu, X. Yuan, Y. Wang, and P. Dai, "Fast model predictive control for multilevel cascaded H-bridge STATCOM with polynomial computation time," *IEEE Trans. Ind. Electron.*, vol. 63, no. 8, pp. 5231–5243, Aug. 2016.

[31] W. Xie *et al.*, "Finite-control-set model predictive torque control with a deadbeat solution for PMSM drives," *IEEE Trans. Ind. Electron.*, vol. 62, no. 9, pp. 5402–5410, Sep. 2015.

[32] I. S. Mohamed, S. A. Zaid, M. F. Abu-Elyazeed, and H. M. Elsayed, "Improved model predictive control for three-phase inverter with output LC filter," *Int. J. Model., Identificat. Control.*, vol. 23, no. 4, pp. 371–379, Apr. 2015.

[33] I. S. Mohamed, S. A. Zaid, M. F. Abu-Elyazeed, and H. M. Elsayed, "Model predictive control-a simple and powerful method to control UPS inverter applications with output LC filter," in *Proc. Saudi Int. Electron., Commun. Photon. Conf.*, 2013, pp. 1–6.

YONG YANG received the B.Sc. degree in automation from Xiangtan University, Xiangtan, China, in 2003, the M.Sc. degree in power electronics from Guizhou University, Guiyang, China, in 2006, and the Ph.D. degree in power electronics from Shanghai University, Shanghai, China, in 2010. He is currently an Assistant Professor with the School of Urban Rail Transportation, Soochow University. He has authored or co-authored over 30 technical papers. His current research interests include distributed energy resource interfacing and control, microgrid, and high-performance motor drive systems.

HUIQING WEN received the B.S. and M.S. degrees in electrical engineering from Zhejiang University, Hangzhou, China, in 2002 and 2006, respectively, and the Ph.D. degree in electrical engineering from the Chinese Academy of Sciences, Beijing, China, in 2009. From 2009 to 2010, he has been an Electrical Engineer with the GE (China) Research and Development Center Company Ltd., Shanghai, China. From 2010 to 2011, he was an Engineer with the China Coal Research Institute, Beijing. From 2011 to 2012, he was a Post-Doctoral Fellow with the Masdar Institute of Science and Technology, Abu Dhabi, United Arab Emirates. He is currently an Associate Professor with Xi'an Jiaotong-Liverpool University, Suzhou, China. His research interests include bidirectional dc–dc converter, power electronics in flexible ac transmission applications, electrical vehicles, and high-power, three-level electrical driving systems.

DEPENG LI received the Ph.D. degree in computer science from Dalhousie University, Canada, in 2010. He is currently an Assistant Professor with the Department of Information and Computer Sciences, University of Hawaii at Manoa. His research interests are in security, privacy, and applied cryptography. His research projects span across areas, such as Internet of Things, smart grids, mobile health-tech, and physical-human-cyber triad.

• • •